

## SPECTRAL LINES FOR POLARIZATION MEASUREMENTS OF THE CORONAL MAGNETIC FIELD. IV. STOKES SIGNALS IN CURRENT-CARRYING FIELDS

P. G. JUDGE, B. C. LOW, AND R. CASINI

High Altitude Observatory, National Center for Atmospheric Research,<sup>1</sup> P.O. Box 3000, Boulder, CO 80307-3000

Received 2006 May 18; accepted 2006 July 19

### ABSTRACT

We present the first theoretical, forward calculations of the Stokes profiles of several magnetic dipole (“M1”) coronal emission lines produced in current-carrying magnetic structures. An idealized coronal model of Low, Fong, and Fan is used, which describes a spherically symmetric, hydrostatic background atmosphere, isothermal at a coronal temperature of  $1.6 \times 10^6$  K. Embedded is a global, axisymmetric magnetic field that is everywhere potential except at a quiescent prominence, consisting of an infinitesimally thin, equatorial current sheet whose weight is supported by the outward discrete Lorentz force in the sheet. This model contains a physically nontrivial, localized magnetic structure, although the atmospheric plasma is thermally of the simplest stratification possible. The calculated M1 coronal lines show clear and distinct signatures of the presence and magnitude of this localized magnetic structure, in both linear and circular polarizations, even though the thermal structure is almost homogeneous. The morphology of maps of linear polarization is particularly sensitive to the existence and strength of the current sheets, as field lines wrap around them according to the Biot-Savart law, and the linear polarization responds to different projections of field line directions onto local radius vectors. Of the M1 lines studied, those of Fe XIII (1074.7 nm) and Si X (1430.1 nm) are especially promising because of their relatively strong linear polarization. These forward calculations provide a basis for optimism that emission-line measurements may reveal the presence and nature of current systems in the corona, and provide motivation for developing instruments capable of routinely measuring polarized light in forbidden coronal lines.

*Subject headings:* polarization — Sun: atmosphere — Sun: corona — Sun: magnetic fields

*Online material:* color figures

### 1. INTRODUCTION

This paper is the fourth in a series devoted to using forbidden emission lines, of magnetic dipole (“M1”) character, to determine properties of coronal magnetic fields. In the first paper (Judge 1998), the visible and infrared coronal forbidden-line spectrum was surveyed and line intensities were calculated for all potentially interesting ions. In the second paper (Casini & Judge 1999) we developed the theoretical framework for the simulation and interpretation of polarized light emitted in M1 coronal lines, extending earlier work (e.g., Sahal-Bréchet 1977) to include consistently the lowest orders in the ratio  $\omega_L/\Delta\omega_D$  (Larmor / Doppler width frequency ratio) needed to model the full Stokes vector. In the corona,  $\omega_L/\Delta\omega_D$  is expected to be  $\sim 10^{-4}$ . Paper III (Brage et al. 2000) dealt with atomic data for M1 lines of Si IX.

The polarized light from M1 lines contains information on coronal magnetic fields of two different kinds. First, the direction of the magnetic field projected onto the plane of the sky is encoded in the observed linear polarization (Charvin 1965). The linear polarization can be relatively large, sometimes approaching tens of percent of the intensity, being essentially independent of  $\omega_L/\Delta\omega_D$ . Second, the strength and sign of the magnetic field along the line of sight (LOS) is encoded in the circular polarization (Harvey 1969; Lin et al. 2000, 2004). This component is generally orders of magnitude smaller, arising mostly from the first-order term in  $\omega_L/\Delta\omega_D$ . The linear polarization arises through the “atomic alignment” (Sahal-Bréchet 1977) produced when typical coronal ions, gyrating around the coronal field lines, are irradiated anisotropically by the solar photosphere. The second

effect is the well-known longitudinal Zeeman effect, but modified in the presence of nonzero atomic alignment (Casini & Judge 1999). Linear polarization arising from the transverse Zeeman effect is negligible, being second order in  $\omega_L/\Delta\omega_D$ , in comparison with the irradiation-induced atomic alignment.

Judge & Casini (2001) discussed the computer program used here for calculating the Stokes profiles of coronal M1 emission lines. There, results were shown for dipolar magnetic field configurations to verify aspects of the program and to illustrate the polarization signatures of simple potential fields. The linear polarization produced by more sophisticated (but still potential) fields, based on surface field extrapolations, received considerable attention in the 1970s and 1980s (e.g., House 1974, 1977), in an effort to see if potential fields approximate actual conditions in the corona. However, practically speaking, potential fields are of limited physical interest because they are at absolutely the lowest energy levels. It is the free energy associated with current systems flowing in the corona that drives the diversity of phenomena we call solar activity, including flares, coronal heating, and large-scale coronal dynamics (e.g., Low 1994). From basic magnetohydrodynamics, Taylor (1986) and Berger (1984) have conjectured that, under conditions of high magnetic Reynolds numbers, magnetic helicity is almost conserved, because it is assumed that the decay time for magnetic helicity greatly exceeds the decay time for magnetic energy. Observations of photospheric magnetic fields have shown that the field that emerges is typically twisted, carrying significant helicity with it (Lites 2005 and reference therein). It follows that even with flaring and magnetic reconnection, the relaxed field cannot reach states that are close to potential under the above approximate conservation law (Low 2003; Zhang & Low 2005). From this physical perspective, the flaring and heating in the corona needed to accommodate the

<sup>1</sup> The National Center for Atmospheric Research is sponsored by the National Science Foundation.

emerging magnetic fields would produce long-lived structures that continue to trap a certain amount of free energy, stored in situ, to be released eventually in coronal mass ejections and their associated flares (e.g., Low 1994).

The broad aim of the present series of papers is to understand the potential capability of M1 emission lines to diagnose coronal magnetic properties using spectropolarimetry. This effort complements more mature work based on radio observations, but whose application is limited to strong-field (i.e., active) regions of the corona (e.g., White 2001). In this paper we take a first step toward understanding the polarimetric signatures of current systems in coronal plasmas. This is accomplished by synthesizing the Stokes signatures of M1 emission lines, in what “may be regarded as the simplest prominence model available in spherical geometry” (Low et al. 2003). The paper has two goals: (1) to predict polarization signatures of the coronal current system in this particular model for comparison with observations, and (2) to examine the sensitivity of the polarization signatures of this physically interesting model, but including the combined complications of a very simple thermal structure and the accompanying LOS integrations. We find it interesting that some robust information on magnetic structures may reside in the polarization signatures despite these complications.

## 2. THE MAGNETIC MODEL

Fong et al. (2002) and Low et al. (2003) developed analytical magnetostatic models of prominences embedded in a corona, in “inverse” configurations (in the sense of Leroy 1989). The models are axisymmetric, and the prominence is treated as a cold plasma sheet forming a flat ring around the Sun, with inner and outer radii at  $r = r_\odot$  and  $r = a > r_\odot$ . The global magnetic field is taken to have a dipolar topology, rooted to the base  $r = r_\odot$ , and potential everywhere, except at the prominence sheet where a discrete azimuthal electric current flows. The magnetic field threads across the prominence sheet with a reversal of the tangential field component to account for the sheet current and a continuous normal component across the sheet to satisfy the solenoidal condition.

With axisymmetry, the solenoidal magnetic field can be expressed in spherical coordinates as

$$\mathbf{B} = \frac{1}{r \sin \theta} \left( \frac{1}{r} \frac{\partial A}{\partial \theta}, -\frac{\partial A}{\partial r}, 0 \right), \quad (1)$$

in terms of a flux function  $A$  (the  $\phi$ -component of the magnetic vector potential). This particular model is attractive for our purpose because the global field can be represented by expressing  $A$  as the sum of just a few oblate spherical harmonic functions  $A_l$ . Each harmonic contributes its share of the azimuthal current in the prominence sheet, permitting some degree of freedom to generate a variety of prominence-embedded global fields. By choosing suitable combinations of  $A_l$  and simple background potential fields, Low et al. showed that the excess weight of prominence material could be balanced by an outward-directed Lorentz force. They focused on the models’ ability to store significant magnetic energy, sufficient to drive coronal mass ejections. In the present paper, the unresolved prominence simply provides weight to balance the Lorentz force. Its presence implies a local torus of closed field around it, distinguishing the global field from a pure dipole potential field. The prominence merely features as the hydromagnetic reason for this interesting magnetic topology but is otherwise irrelevant. The surrounding coronal material is of central interest here, as it emits polarized light in certain M1 emission lines.

Following the notation of Fong et al. (2002) and Low et al. (2003), consider the flux function

$$A_{\text{sheet}} = B_\odot r_\odot^2 (A_3 - A_l), \quad (2)$$

where  $A_3$  is the third spheroidal harmonic function and  $A_l$  is its image flux function, such that  $A_l$  is everywhere potential in  $r > r_\odot$  and with  $A_l(r_\odot) = A_3(r_\odot)$ . Using equations (1) and (2), the latter condition implies that the current sheet contributes zero radial field component at  $r = r_\odot$ . The potential field  $A_l$  was computed as a truncated series expansion of solutions to Laplace’s equation using associated Legendre polynomials, subject to matching  $A_l$  at  $r = r_\odot$  with  $A_3(r_\odot)$ . The flux function  $A_{\text{sheet}}$  accounts for the field due to the prominence current sheet. Our total flux function is then the sum of  $A_{\text{sheet}}$  and that for a potential field,  $A_{\text{dip}}$ , which accounts for the global surface field at  $r = r_\odot$ :

$$A = A_{\text{dip}} + \gamma A_{\text{sheet}}, \quad A_{\text{dip}} = B_\odot r_\odot^3 \frac{\sin^2 \theta}{r}. \quad (3)$$

As  $\gamma$  is varied, the coronal magnetic field and embedded prominence sheet change, but the radial component of the surface magnetic field  $B_r(r = r_\odot)$  remains unchanged. This property is important because on the real Sun, current systems in the corona cannot significantly affect the magnetic fields in the far denser, highly conducting surface layers.

Furthermore, one might envisage making the usual potential field extrapolations based on measurements of  $B_r(r = r_\odot)$  (e.g., Altschuler & Newkirk 1969). Since  $A_l(r_\odot) = A_3(r_\odot)$ , such an extrapolation will recover only the potential field due to the  $A_{\text{dip}}$  term alone, a pure dipole potential field, and miss the non-dipolar magnetic structure arising from the prominence current sheet in the corona. By varying  $\gamma$ , we can effectively study the influence of an in situ prominence current sheet on the polarization of M1 lines, detecting a magnetic structure missed by the potential-field extrapolation from the surface fields. We thus have an instructive example of how the emission-line polarization may contain information on a current system in the corona, which is “invisible” to potential extrapolations based on surface magnetic fields.

Outside of the (infinitesimally thin) current sheet, the magnetic field is potential and so a spherically symmetric corona must obey the hydrostatic relationship

$$\frac{dp}{dr} + \rho \frac{GM_\odot}{r^2} = 0. \quad (4)$$

We assume the corona is fully ionized and is at a temperature of 1.6 MK, chosen to be close to the peak formation temperature of two Fe XIII lines of particular interest near 1074.7 and 1079.8 nm. The pressure at  $r = r_\odot$  was set to 0.14 dynes  $\text{cm}^{-2}$ . These values are typical of the quiet corona (e.g., Billings 1966). Note that outside of the current sheet, the force balance of the magnetic field is decoupled from that of the plasma. The only departure of the field from a potential state arises within the current sheet, which contributes nothing to our coronal emission line calculations.

The axisymmetric magnetic fields of Low et al. (2003) are arguably the simplest magnetostatic configurations with embedded electric currents one expects to find in the corona. The adopted thermal structure is simpler yet, being spherically symmetric and isothermal, and is the simplest model compatible with gravitational stratification. The high degree of symmetry in the thermal structure is radically different from the fine structures organized into loops and rays that are prominent in EUV images (e.g., Golub et al. 1999). Our purpose here is not to try to study such complex

configurations, which are associated with magnetic complexity on small ( $\ll r_\odot$ ) spatial scales, but instead to examine the polarization signatures of the magnetic structure in the large scale “diffuse” corona. Furthermore, our calculations represent cases where contributions to the LOS integration of emission coefficients come from very large volumes.

Since prominences are rarely aligned exactly along lines of constant latitude, the computations were made with the south pole of the axis of symmetry tilted along the solar east-west axis by  $7^\circ$  toward the “observer.” This breaks the symmetry in the calculation of the Stokes  $V$ , which otherwise would be identically zero. We could have chosen a variety of tilt angles; we chose  $7^\circ$  simply because it corresponds to the maximum tilt (solar “ $b$ -angle”) as seen from the Earth.

In the models of Low et al. (2003) the weight of a prominence balances the upward Lorentz force within the current sheet. The presence of the prominence in the atmosphere therefore has two consequences. The support of its weight requires, in this model, a local magnetic structure in the form of a torus of closed field around the prominence. The weight also stresses the field in this cavity and its surroundings, building up magnetic energy stored in the atmosphere. The values of  $\gamma$  thus determine the prominence mass, which for  $\gamma = 0.042$  and a prominence of length  $r_\odot$  is around  $10^{17}$  g. This is far larger than a recent determination of  $(6 \pm 2.5) \times 10^{14}$  g for a CME-associated eruptive prominence (Gilbert et al. 2005). Low et al. (2003) recognized the relatively large mass and so made calculations in a different configuration in which a “flattened dipole” field was used with weaker equatorial fields than that adopted here, leading to a smaller prominence mass by a factor of 4. Although the prominence mass determined by Gilbert et al. is small, larger values of prominence mass of the order of  $10^{15}$ – $10^{16}$  g have been cited in the literature (Illing & Hundhausen 1986; Gopalswamy & Hanaoka 1998). The issue of prominence mass is important for understanding energy storage but is not vital to the present study concerned with the signatures of coronal currents in polarized light, irrespective of their physical origin.

### 3. EMISSION-LINE CALCULATIONS

We performed calculations of emission coefficients using the formalism described by Casini & Judge (1999) as written into the computer program discussed by Judge & Casini (2001). A uniform Cartesian grid was used, the grid points being 2.9 Mm ( $4''$ ) apart. This spacing was chosen to approximate the  $4''$  pixel sizes of the CoMP instrument (Darnell et al. 2003; Tomczyk 2003), as it has been implemented on the “One Shot” coronagraph (Smart et al. 1981) at the National Solar Observatory on Sacramento Peak. For each grid point, emission coefficients for each Stokes component ( $I$ ,  $Q$ ,  $U$ ,  $V$ ), evaluated along the LOS, are computed by solving the statistical equilibrium equations for a given ion. The equations are written in terms of the components of the irreducible spherical components of the density matrix, which, in the absence of atomic coherences, is equivalent to the formalism based on the magnetic substate populations (House 1977). Along each LOS the four emission coefficients corresponding to  $I$ ,  $Q$ ,  $U$ , and  $V$  were integrated using the trapezoidal rule. A fifth emission coefficient for  $V$  was computed in which the contribution of atomic alignment at each grid point was set to zero [ $\sigma_0^2(\alpha_0, J_0) = 0$  in eq. (35c) of Casini & Judge 1999]. This gives the Stokes  $V$  profile expected from application of the well-known magnetograph formula.

Calculations were performed for several different ions of potential interest, with special emphasis on the Si-like ion Fe XIII, whose well-known infrared transitions have been the subjects of

many coronagraphic studies (e.g., Querfeld 1977, 1982; Querfeld & Smartt 1984; Arnaud & Newkirk 1987; Lin et al. 2000, 2004; Tomczyk et al. 2004; Tomczyk 2004). We present results using a three-level atom for Fe XIII, which contains just the  $3s^2 3p^2 \ ^3P_{0,1,2}$  levels needed to describe the 1074.7 nm ( $J = 1 \rightarrow 0$ ) and 1079.8 nm ( $J = 2 \rightarrow 1$ ) M1 transitions primarily of interest. Using just three levels substantially underestimates the influence of excitation to and radiative cascade from higher lying levels (e.g., Sahal-Br  chot 1974a, 1974b, 1977). In the Appendix, we show how collision rates can be modified in a three-level atomic model roughly to mimic the excitation/cascade effects in models containing many more levels. Atomic models for ions of Fe X, Fe XIV, Si IX, and Si X were treated in a similar fashion. These ions were deemed of particular interest by Judge et al. (2001) since they contain promising M1 lines: the “red” and “green” coronal lines, and lines at 3934.6 and 1430.1 nm, respectively.

Solar abundances are currently under debate. We adopted abundances of iron and silicon of 7.60 and 7.52, respectively, on the logarithmic scale where the hydrogen abundance is 12 (Allen 1973). Recent work yields 7.45 and 7.51, respectively (Asplund et al. 2005). Thus we may overestimate all the Stokes parameters for iron lines by a factor of 1.4. This is of no concern to the present paper, whose conclusions hinge on morphology of the Stokes parameters and ratios of Stokes parameters, independent of their absolute values.

## 4. RESULTS AND DISCUSSION

Stokes parameters were calculated for three magnetic configurations, each with identical thermal properties. The three models differ only in their embedded magnetic fields, simply by changing the value of  $\gamma$  in equation (3) from zero (pure dipolar field) to 0.024 and 0.042. The latter values were chosen following § 3.1 of the paper by Low et al. (2003; see their Figs. 1 and 2):  $\gamma = 0.042$  has sufficient magnetic free energy to allow both opening of the field lines and also to drive a CME related outflow under typical conditions. This free energy is actually among the largest of energies of observed CME/flare events (Low et al. 2003). On the other hand, the case  $\gamma = 0.024$  has insufficient energy to permit field line opening and CME eruption:  $\gamma = 0.024$  is  $0.042/\sqrt{3}$ , and so the  $\gamma = 0.024$  case has one-third of the free energy of the 0.042 case;  $\gamma = 0.024$  is also roughly the smallest value that can maintain an upward-directed Lorentz force (see the small closed loop at the top of the current sheet in Fig. 1b). These two cases therefore serve to address the following questions: *Do Stokes parameters of M1 lines reflect the presence of current sheets in the corona, and can they be used to discriminate between idealized field configurations known to have sufficient/insufficient free energy to launch a CME?*

We note that the thermal structure, being spherically symmetric and hydrostatic, in a sense maximizes the “blurring” effect of LOS integrations on the emergent Stokes profiles, because the profiles have contributions from a broad region centered about the plane of the sky. In the real corona, LOS integrations will have contributions from denser concentrations of coronal material along the LOS, from loops perhaps, hopefully leading to less LOS blurring. However, these concentrations may be associated with separate magnetic structures, confusing the interpretation.

### 4.1. Lines of Fe XIII

Figure 1 shows how the linear polarization, integrated over the line profile of the 1074.7 nm line of Fe XIII, responds to changing the value of  $\gamma$  in equation (3), from a pure dipole field ( $\gamma = 0$ ), to 0.024, and to 0.042. The current sheets are clearly imprinted in a characteristic fashion on the emitted linear polarization. The

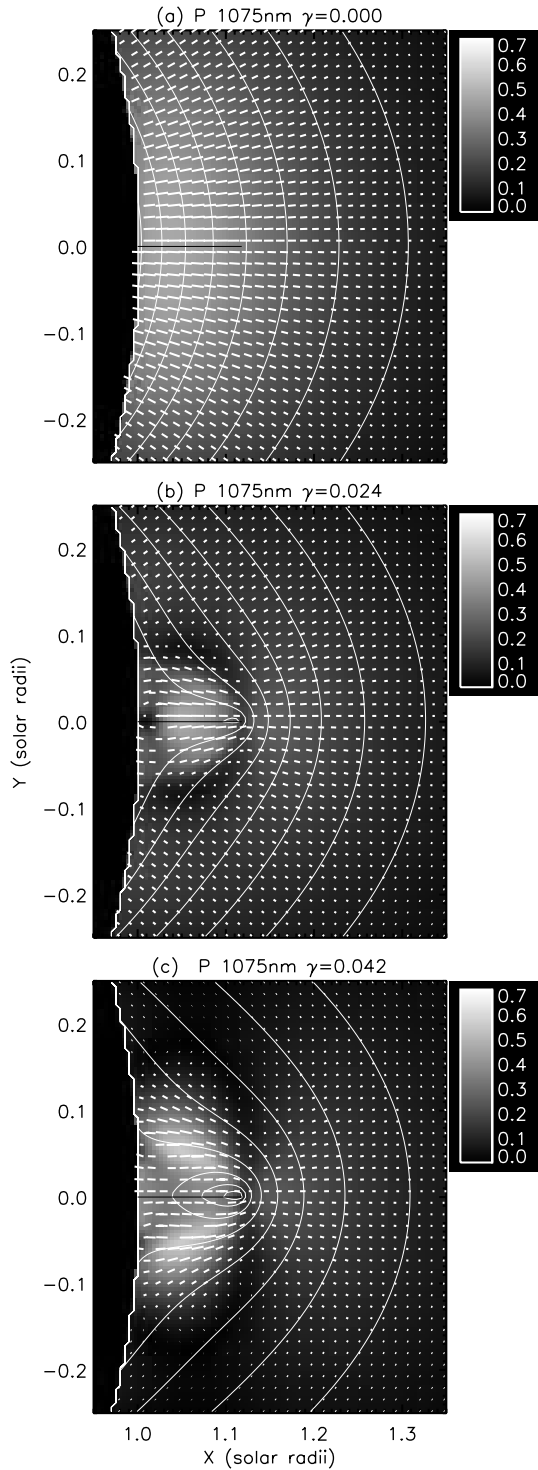


FIG. 1.— Comparison of three calculations of linear polarization in the 1074.7 nm transition of Fe XIII. The strength of the axial current sheet increases from top ( $\gamma = 0$ ) to bottom ( $\gamma = 0.042$ ). The image brightness shows the magnitude of linear polarization  $P = (Q^2 + U^2)^{1/2}$ ; the short lines show the direction of the electric field vector in the plane of the sky (the field “azimuth”). The curved lines are magnetic field lines in the plane of the sky. [See the electronic edition of the *Journal* for a color version of this figure.]

patterns seen in Figures 1b and 1c can be understood through the well-known “Van Vleck effect,” in which zeros of  $P = (Q^2 + U^2)^{1/2}$  are found at locations where the angle  $\vartheta_B$  between the local magnetic field and radius vector (the vector whose origin is at the Sun center) satisfies  $3 \cos^2 \vartheta_B - 1 = 0$ . On opposite

sides of these polarization “nulls,” the electric vector of the polarized light changes direction by  $90^\circ$ . This effect is illustrated in Figures 1b and 1c by the darkest regions surrounding the current sheets: below the dark region (a polarization null) the polarization vectors are parallel to the magnetic field lines; above it they are perpendicular. Thus, the figure shows that the morphology of the images in linear polarization mainly reflect the variation of  $\vartheta_B$  as the magnetic field changes direction in response to the current sheet. The field lines, in the  $\gamma = 0.042$  (strong current) case, wrap around and through the current sheet in accordance with the Biot-Savart law. The differences between the three cases thus directly reflect the magnetic field direction, projected onto the plane of the sky. The magnitudes  $P$  of linear polarization are less directly related to simple coronal properties, because they are determined by the balance between the radiative atomic alignment process arising from the anisotropic irradiation of the ions, and the (assumed isotropic) collisional processes that destroy the atomic alignment. The latter depend on the details of the statistical equilibrium in a multilevel situation and have no simple interpretation (see the Appendix).

In a similar manner to Figure 1, Figure 2 shows how the circular polarization of the 1074.7 nm line responds to the current sheet. The  $V$  profiles change sign with wavelengths  $\lambda$  above and below line center  $\lambda_0$ , so the figure shows  $V = \int V_\lambda S_\lambda d\lambda$ , with  $S_\lambda = \text{sgn}(\lambda - \lambda_0)$ , divided by  $I = \int I_\lambda d\lambda$ . These  $V$  data are non-zero only because of the small polar axis tilt that breaks the LOS symmetry (§ 2). The emission coefficient for  $V$ , given by equations (40) and (41) of Casini & Judge (1999), has a leading term that is independent of the atomic alignment and that corresponds to the well-known weak-field limit (magnetograph formula) for the Zeeman effect. The alignment appears as corrections to the magnetograph formula, which for the case of Fe XIII 1074.7 nm is typically 23%, and is less in the presence of collisions (see the discussion following eq. [41] of Casini & Judge 1999). Thus, the  $V/I$  data shown in Figure 2 reflect largely the magnetograph regime: the tilted dipole has a small  $V$  signature owing to the dipolar tilt, and the data neighboring the current sheet show the signatures of the tilted stronger fields that, in Figure 2c, circulate around the sheet.

The departure of the  $V$  data from the magnetograph formula is illustrated in Figure 3a. The median value of the ratio (magnetograph formula)/(full formula) for this figure is 1.03. Figure 3 also shows the ratios of the intensities  $I$  and linear polarization  $P$  of the 1079.8 nm line to those for the 1074.7 nm line. Median values are respectively 0.30 and 0.024. The intensity ratio is sensitive to both the incident radiation field and the electron density (Flower & Pineau des Forêts 1973). The radiation field is determined by photospheric light and so can be estimated from observations. Given this radiation field, the mean electron density along the LOS can then be determined. Penn et al. (1994) obtained data for the 1079.8 and 1074.7 nm lines from the 1991 total eclipse, and inferred reasonable values for the electron densities. Their observed line intensity ratio (1079.8 nm/1074.7 nm) varied from 0.4 to 0.25 between 1.03 and 1.13  $r_\odot$  above the limb. Our simulated intensity ratios are in excellent agreement with the magnitude and variation with height of these observations. It will be interesting to examine new data from the CoMP instrument (Darnell et al. 2003; Tomczyk 2003), including the magnitudes of linear polarization in the two lines.

Note that the circular polarization arising from the two current sheet models differs essentially only in its magnitude (Fig. 2). However, the linear polarization in these calculations is strikingly sensitive to the presence and strength of the fields generated by the current sheet (Fig. 1). Both magnitudes and field azimuths

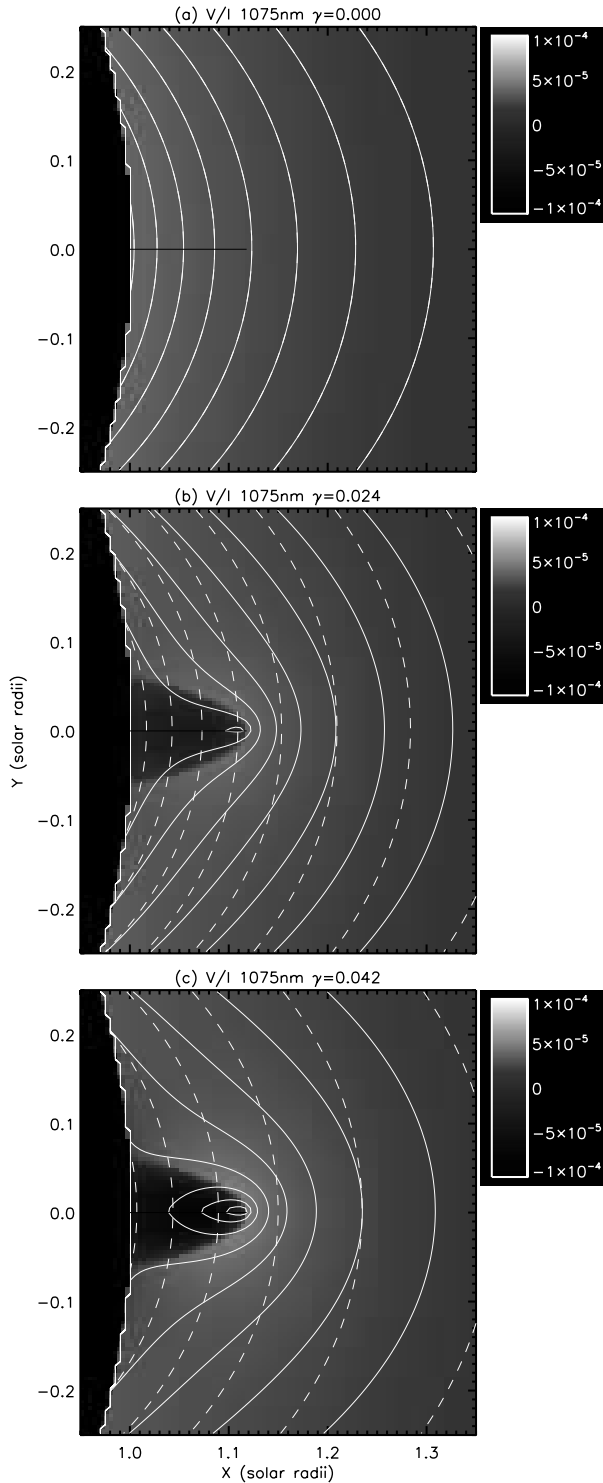


FIG. 2.—Comparison of three calculations of circular polarization, plotted as in Fig. 1. Dashed lines show the magnetic field lines of the dipolar field only, for comparison. [See the electronic edition of the Journal for a color version of this figure.]

differ dramatically between the  $\gamma = 0.024$  and  $\gamma = 0.042$  cases, in response to the changes in field line morphology, as a result of the dependence of the linear polarization vectors on  $\vartheta_B$ . Therefore, considerable emphasis should be placed on interpreting *linear* as well as circular polarization signals of M1 lines, when attempting to diagnose current systems and the associated magnetic free energy within the corona. The linear polarization maps are essen-

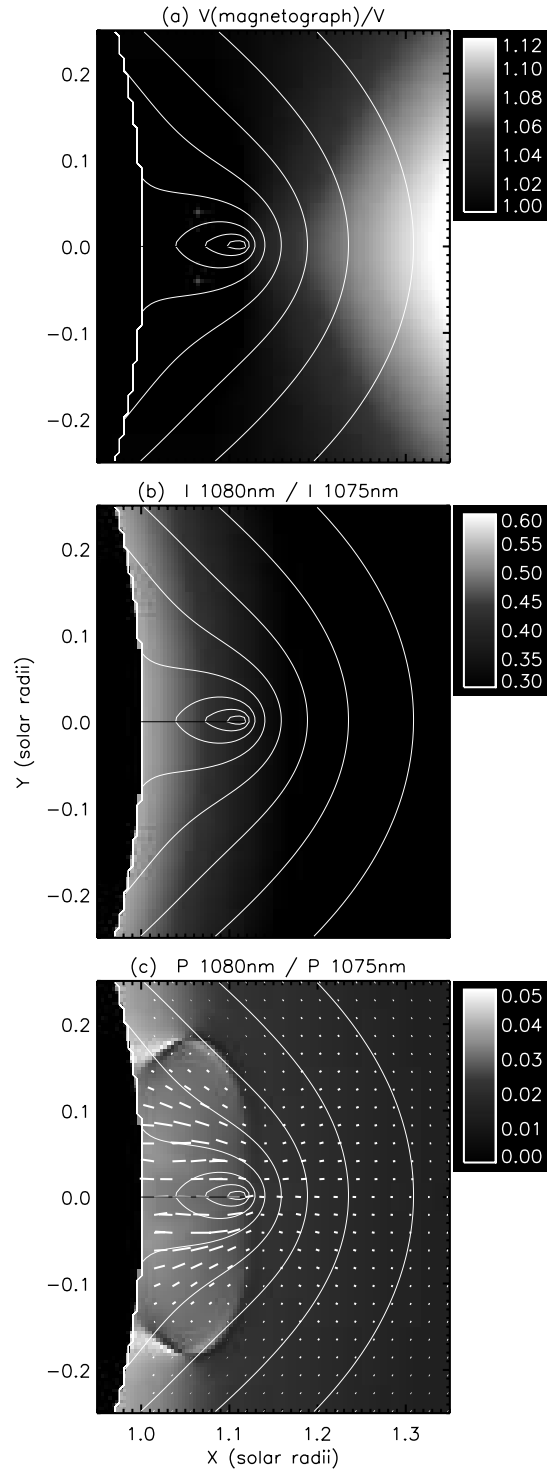


FIG. 3.—(a) Ratio of the Stokes  $V$  data for the 1074.7 nm line computed using the “magnetograph formula” (eq. [40] of Casini & Judge 1999) to the calculation including the correction for atomic alignment. (This ratio is  $1/\kappa$  given by Casini & Judge 1999). (b) Ratio of the intensities of the 1079.8 and 1074.7 nm lines. (c) Ratio of the magnitudes of the linear polarization of the same lines. The data in (b) and (c) can be usefully compared with observational data. [See the electronic edition of the Journal for a color version of this figure.]

tially unaffected by the magnitude of the magnetic field. This is because the lines form in the “strong field” limit of the Hanle effect ( $\omega_L \tau \gg 1$ , where  $\tau$  is the radiative lifetime of the upper level of the line). In our calculations these maps are therefore dependent only on the values of  $\gamma$  and not on the absolute values

TABLE 1  
A COMPARISON OF POLARIZATION PROPERTIES FOR SEVERAL M1 LINES

Ion	$\lambda$ (nm)	$I$ (ergs cm <sup>-2</sup> s <sup>-1</sup> sr <sup>-1</sup> )	$P/I$	$ V/I $
Fe XIII .....	1074.7	1.05E1	4.2E-2	2.9E-5
	1079.8	4.68E0	2.9E-3	2.8E-5
Si IX .....	3934.6	1.97E-1	2.0E-3	7.9E-5
Fe X .....	637.4	4.48E-1	0.00E0	1.6E-5
Fe XIV .....	530.3	6.50E0	8.3E-3	1.4E-5
Si X .....	1430.1	2.95E0	1.6E-2	2.9E-5

NOTES.—These results are for  $x = 1.07 r_{\odot}$ , averaged over several points between  $y = -0.05$  and  $+0.05 r_{\odot}$  in Figs. 1–3.

of the magnetic fields. Thus, these maps alone cannot determine the magnitudes of the magnetic field, the free magnetic energy density, or the electric currents. To measure the currents themselves, the magnitude of the magnetic field is needed, which requires interpretation of the circular polarization. The point we make here is that in the context of the adopted models, the maps of linear polarization can nevertheless be used to discriminate between two physically interesting cases with and without sufficient free energy to launch a CME.

#### 4.2. Lines of Fe X, Fe XIV, Si IX, and Si X

Judge et al. (2001) assigned a “figure of merit” to a variety of M1 coronal lines based on an estimate of the photon-limited signal-to-noise ratio of the circular polarization in the lines. The calculations for Fe XIII presented here show that, at least for one simple current system, the linear polarization can play a critical role in identifying the presence and relative strength of electric currents in the corona. Therefore, we have calculated the Stokes profiles of M1 lines of Fe X (637.4 nm), Fe XIV (530.3 nm), Si IX (3934.6 nm), and Si X (1430.1 nm), the most promising M1 lines listed in Table 8 of Judge et al. (2001). We excluded Mg VIII because the M1 line near 3027 nm suffers from significant telluric absorption.

Results for a representative point  $0.07 r_{\odot}$  above the solar limb are listed in Table 1, for the case where  $\gamma = 0.042$ . The computed circular polarization signals are similar to those calculated above for Fe XIII, scaled by  $\lambda g$ , where  $\lambda$  is the wavelength and  $g$  is the Landé  $g$ -factor of the transition. As expected, the  $|V/I|$  ratios were largest for the 3934.6 nm line of Si IX, and smallest for Fe XIV 530.3 nm. The linear polarization results are more interesting. The upper level of Fe X 637.4 is “unpolarizable,” being a  $J = 1/2$  level, and the line has no linear polarization. The most Zeeman-sensitive line, that of Si IX 3934.6 nm, has a very small  $P/I$  as a result of the relative dominance of electron collisions over photoexcitation. This situation arises because the Sun’s photosphere is dimmer near  $4 \mu\text{m}$ , because the Einstein coefficients scale with  $\lambda^{-3}$  for dipole transitions, and because collision rates are generally larger for ions with lower charge (the scale of radial wave functions varies with core charge  $z$  as  $z^{-1}$ ; hence cross sections scale with  $z^{-2}$ ). The Mg VIII M1 line near 3027 nm is expected to behave similarly to that of Si IX. Of the remaining lines, that of Si X at 1430.1 nm behaves similarly to Fe XIII, and the “green” line at 530.3 nm is characterized by  $P/I$  on the order of 1% or less. These results are broadly consistent with the earlier calculations made for Fe XIII and Fe XIV by, e.g., House (1977) and Sahal-Br  chot (1977).

#### 5. CONCLUSIONS

Polarization observations of M1 coronal lines can indeed indicate current sheets in the corona, and in this particular case can

also discriminate between idealized field configurations known to have sufficient/insufficient free energy to launch a CME. Salient properties of our particular current sheets are reflected most sensitively by the linear polarization signatures of M1 lines, as field lines wrap around the electrical currents according to the Biot-Savart law, and the linear polarization responds to the different projection of field line directions onto the local radius vector. Combined with intensity and circular polarization measurements, the presence of such a large scale current system in the real solar corona should be discernible and should be sought, for example, in prominence cavity data in the future. Together with models, it is hoped that one might be able to limit and/or measure the free energy associated with certain polarization data, and determine the likelihood of CME eruption, for example. This task is beyond the scope of the present paper, but is under study.

Our emphasis on the linear polarization reflects to some degree our assumed geometry, in which currents flow largely along the LOS. Nevertheless, linear polarization measurements offer a more general opportunity for diagnosis of coronal current systems because the field line morphology determined by the currents is imprinted in images of the linear polarizations of M1 lines, including the nulls in the linear polarization and the  $90^\circ$  change in polarization direction across these nulls: the Van Vleck effect. We anticipate, for example, that current-carrying fields in the “normal” and “inverse” prominence configurations modeled by Zhang & Low (2004) will have very different polarization signatures (on the basis of the field line morphology shown in their Fig. 2). These two types of configurations, originally proposed on the basis of magnetic field measurements in prominence plasma (e.g., Leroy 1989), may therefore be more directly tested observationally over the entire hydromagnetic structure.

In the past the Van Vleck effect has been regarded as a troublesome source of ambiguity. However, the striking differences between the images shown in Figure 1 suggest that the morphology of linear polarization maps including the Van Vleck effect may actually *help* disentangle the field morphology. To some degree this idea was anticipated 34 years ago by House (1972): “It appears that it will be most important to have polarization measurements over a large region of the corona so that through the continuity of the field one may attempt to resolve some of the ambiguities.”

Work is in progress at the High Altitude Observatory and the Universities of Hawaii and Michigan to analyze data from new instruments and to develop a new coronagraphic instrument devoted to synoptic measurements of the polarization of M1 coronal lines. Given the clear importance of the linear polarization measurements in detecting coronal current systems, such an instrument should measure lines with significant linear polarization signatures, giving more weight to the lines of Si X, Fe XIII, and Fe XIV than Si IX and Fe X, in spite of the large magnetic sensitivity of the Si IX line at 3934.6 nm. Such a synoptic instrument must obtain useful data throughout the solar cycle, and perhaps within coronal holes. Billings (1966) has reviewed the dependence of M1 line intensities over the sunspot cycle. The red Fe X line can be detected throughout the sunspot cycle, the green Fe XIV line has a strong cyclic dependence, and the yellow Ca XV line is only associated with sunspots. S. Tomczyk (2005, private communication) has noted that Fe XIII is faint during the present sunspot minimum. The line of Si X at 1430.1 nm, which has qualitatively similar computed values of  $Q$ ,  $U$ , and  $V$  to those of Fe XIII 1074.7 nm, may be expected to remain bright throughout the solar cycle since it has a much higher ionic abundance near  $10^6$  K than Fe XIII (e.g., Jordan 1969; Arnaud & Raymond

1992). The temperature-dependent ionization equilibrium fraction of Si x lies closer to that of Fe x than that of Fe xiii. The Si x line appears free from significant telluric absorption and is of the same order of brightness as computed here (Penn & Kuhn 1994). These considerations point to an instrument capable of measuring at least the lines of both Fe xiii and Si x, if observational con-

straints on the free energy associated with coronal current systems are desired.

We are grateful to Sarah Gibson for a careful reading of the paper.

## APPENDIX

### EFFECTS OF EXCITATION TO LEVELS ABOVE $3s^23p^2\ ^3P_{0,1,2}$ IN Fe xiii

Polarization calculations were made using atomic models of a various levels of sophistication. Those reported in the text used the simplest possible model, modified as described below, including just the three lowest levels ( $\ ^3P_{0,1,2}$ ) of the Fe xiii ion. The modifications were made based on calculations in a 27 level atomic model for which accurate rate coefficients are available (Dere et al. 2001).

Restriction to a small number of levels is questionable, as was demonstrated for the case of Fe xiv by House (1974). Under coronal conditions it is well known that both level populations (Pecker & Thomas 1962) and magnetic sublevel populations (Sahal-Bréchet 1974a, 1974b, 1977) are controlled by electron impact excitation to, and radiative decay from, higher levels. Our restriction to three levels is dictated by excessive computer time with the current version of the code. To set up and solve the statistical equilibrium equations for the population, alignment and orientation of each of 27 levels requires roughly 0.9 s on a 1.8 GHz, single-processor PowerPC iMac. With an excess of 2 million grid points just one such calculation requires 29 days. We therefore made an exploratory set of calculations using the 27 level model from the CHIANTI package. The model includes the lowest five levels of even parity ( $\ ^3P_{0,1,2}$ ,  $\ ^1D_2$ ,  $\ ^1S_0$ , all of the ground  $3s^23p^2$  configuration), which were treated by Sahal-Bréchet (1977). Twenty-two levels of odd parity, readily populated by thermal electrons, were also included for which data for radiative and electron collisional transitions are available ( $\ ^5S_2^o$ ,  $\ ^3P_{0,1,2}^o$ ,  $\ ^3D_{1,2,3}^o$ ,  $\ ^1D_2^o$ ,  $\ ^3S_1^o$ ,  $\ ^1P_1^o$ , all levels of the  $3s3p^3$  configuration lying between 26 and 54 eV above the ground level;  $\ ^3D_{1,2,3}^o$ ,  $\ ^3F_{2,3,4}^o$ ,  $\ ^3P_{0,1,2}^o$ ,  $\ ^1D_2^o$ ,  $\ ^1F_3^o$ ,  $\ ^1P_1^o$  levels of the  $3s^23p3d$  configuration, lying between 53 and 71 eV). These levels were also treated by House (1977). Oscillator strengths and collisions between levels with quantum numbers  $\alpha'J'$  to  $\alpha J$  by electron impact were taken from the CHIANTI project (Dere et al. 2001). For completeness, inelastic and elastic collisions by proton impact between substates of the three lowest levels were included, assuming equal proton and electron temperatures. These data were taken from Landman (1975), although Sahal-Bréchet (1977) found them to have a small effect when proton and electron temperatures are similar.

Our treatment of impacts by electron collisions involves some approximations that need explanation. It is based on the treatment described in Appendix A4 of Landi degl'Innocenti & Landolfi (2004). The characteristics of inelastic and superelastic electron-ion collisions are reviewed by Burgess & Tully (1992). We assume Maxwellian electron distributions. For electric dipole and quadrupole (E1 and E2) transitions, we assume that the collisional rate coefficients are dominated by the multipolar interaction between the collider and target atom, and compute the inelastic and superelastic collisional rates needed for the equilibrium calculations assuming (1) that no other multipoles contribute, and (2) that the effects of resonances (doubly excited intermediate ionic states of Fe xiii) are negligible. This is generally a good approximation for such transitions. For otherwise forbidden transitions, we make the opposite assumption, namely, that the multipolar interaction is negligible compared with the interactions that occur as the colliding electron interacts strongly with the bound electrons. Under this approximation, the “strong coupling” case, there is no preferred orientation and so we set the desired inelastic collision rates between magnetic substates from level  $\alpha_l J_l$  to  $\alpha J$  ( $l$  refers to the energetically lower level), as

$$C(\alpha J M, \alpha_l J_l M_l) = C(\alpha J, \alpha_l J_l) / (2J_l + 1) \quad (\text{forbidden transitions}). \quad (\text{A1})$$

As described in the Appendix A4 of Landi degl'Innocenti & Landolfi (2004) the coefficients for the E1, E2 transitions and the forbidden transitions are used to compute coefficients  $\Gamma_I^{(\tilde{K})}(\alpha J, \alpha_l J_l)$  (and similarly for  $\Gamma_S$ ) for multipole order  $\tilde{K}$  needed for computation of rate coefficients in the basis of irreducible spherical tensor operators adopted by Sahal-Bréchet (1977) and Casini & Judge (1999).

Figure 4 compares intensities of the 1074.7 and 1079.8 nm M1 lines of Fe iii computed using the 27 level atom and using the three-level atom. The three-level atom was treated in two ways: first, the model was run with no modification, revealing gross discrepancies with the “realistic” 27 level model. Second, the collisional rates between the three  $\ ^3P_{J=0,1,2}$  levels were arbitrarily adjusted to see if the “realistic” intensities could be reproduced in a three-level model. The figure shows, fortuitously, that this is indeed the case. The modified three-level atom has collisional rates in the 0–1, 0–2, and 1–2 transitions multiplied by factors of 7.5, 9.4, and 9.4, respectively. The figure shows that this modification mimics the “realistic” calculation quite accurately.

Cross sections for collisions that induce non- $J$ -changing transitions (“elastic” collisions) are unavailable for Fe xiii, except for the proton rates computed by Landman (1975). Such collisions depolarize the atomic levels and hence their emitted radiation. As in earlier work (e.g., Sahal-Bréchet 1977), we assume that these collisional rates are unimportant compared with the large collisional rates associated with the E1 transitions. However, since the levels accessible to E1 transitions from the ground levels of Fe xiii are not present in the three-level atom, the three-level atom therefore misses important sources of depolarization. In order to approximate the effects of multilevel depolarization including E1 transitions, we therefore have adjusted a parameter defined as  $C_E^{(0)}(\alpha J)$  by Landi degl'Innocenti & Landolfi (2004) to try to mimic the depolarization effects of the missing higher atomic levels. By trial and error we found that a value of  $C_E^{(0)}(\alpha J) = 9 \times 10^{-9} \text{ cm}^{-3} \text{ s}^{-1}$  was needed to reproduce the results from the 27 level atom (see Fig. 5, which compares, in a similar fashion to Fig. 4, the magnitude of linear polarization computed in the 1074.7 and 1079.8 nm M1 lines of Fe xiii). The figure shows that this modification reproduces the “realistic” calculation again quite accurately, and sufficiently for the purposes of the present work.

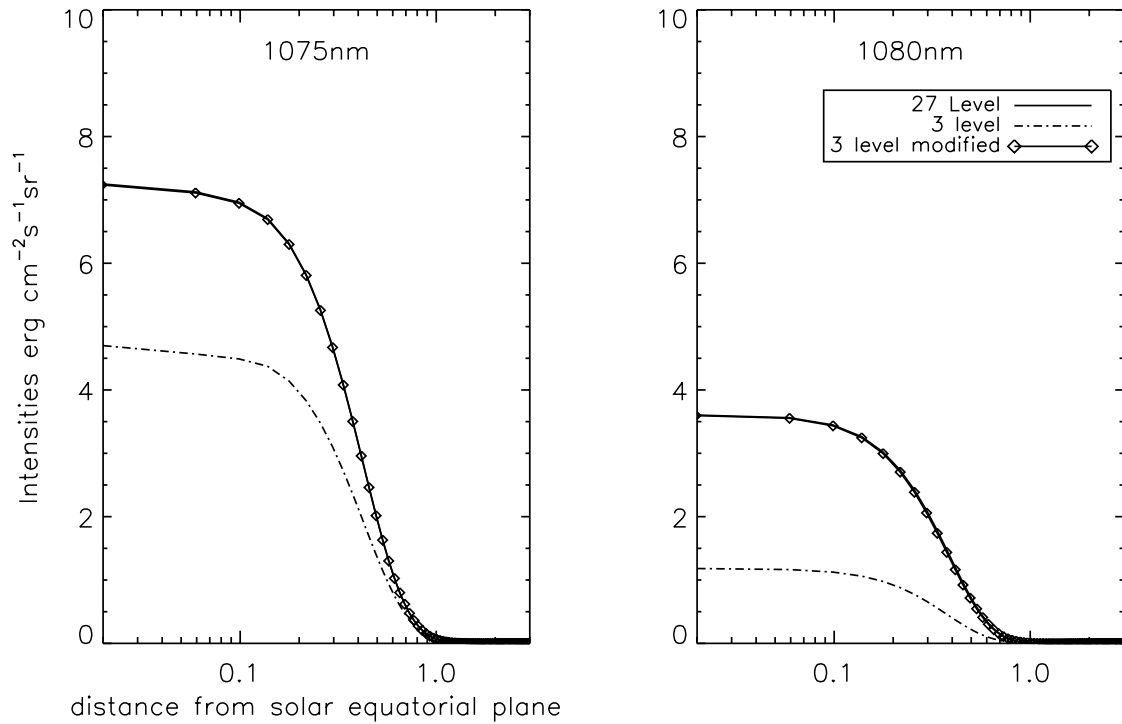


FIG. 4.—Three calculations of line intensities as computed along a north-south (solar  $y$ ) strip of  $3 r_{\odot}$  length starting from the equator, beginning at a distance of  $x = 1.05 r_{\odot}$  from Sun center. The unmodified three-level atom fails to reproduce line intensities by a large margin because of multilevel effects described in the Appendix. By simple trial-and-error modifications of the rates of inelastic electron collisions, the three-level calculation can be brought into very close agreement with the 27 level model.

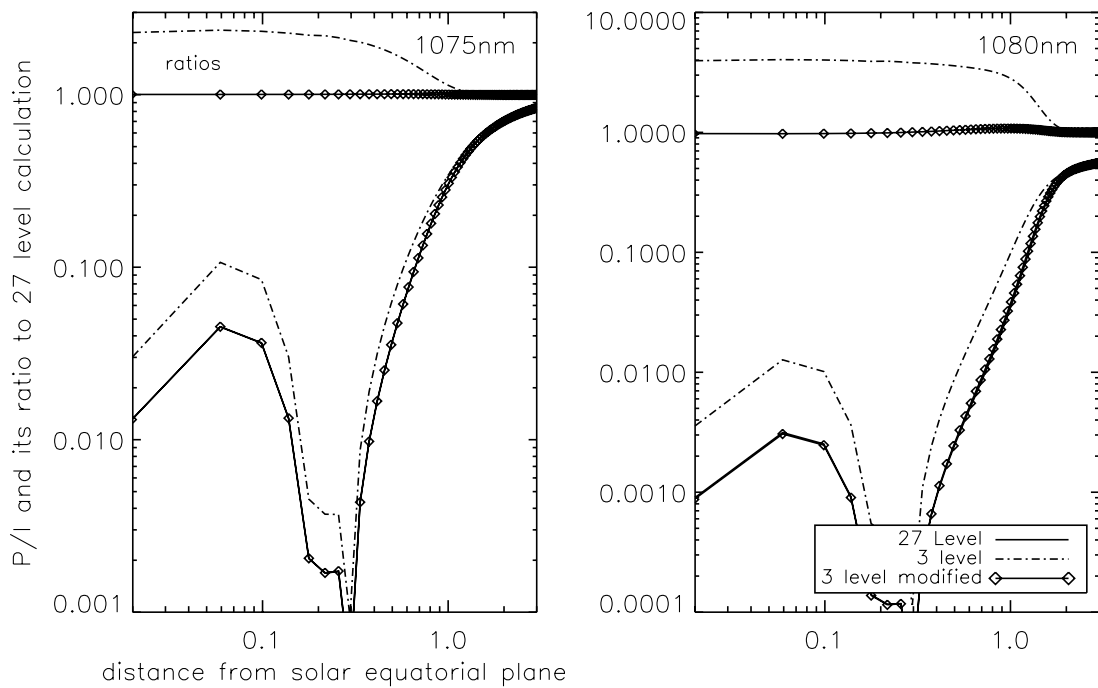


FIG. 5.—Three calculations of linear polarization as computed along the same north-south strip computed in Fig. 4. The unmodified three-level atom greatly overestimates the linear polarization when collisions are important, a well-known result of missing multilevel effects from higher levels (see text). By artificially increasing the elastic rate of electron collisional depolarization, the excitation/cascade depolarization effects can be mimicked for the 1074.7 and 1079.8 nm lines to within a few percent in these calculations.

## REFERENCES

- Allen, C. W. 1973, *Astrophysical Quantities* (London: Athlone Press)
- Altschuler, M. D., & Newkirk, G., Jr. 1969, *Sol. Phys.*, 9, 131
- Arnaud, J., & Newkirk, G., Jr. 1987, *A&A*, 178, 263
- Arnaud, M., & Raymond, J. 1992, *ApJ*, 398, 394
- Asplund, M., Grevesse, N., & Sauval, A. J. 2005, in *ASP Conf. Ser.* 336, *Cosmic Abundances as Records of Stellar Evolution and Nucleosynthesis*, ed. T. G. Barnes, III, and F. N. Bash (San Francisco: ASP), 25
- Berger, M. A. 1984, *Geophys. Astrophys. Fluid Dyn.*, 30, 79
- Billings, D. E. 1966, *A Guide to the Solar Corona* (New York: Academic Press)
- Brage, T., Judge, P. G., Joensson, P., & Edwards, D. P. 2000, *ApJ*, 540, 1114
- Burgess, A., & Tully, J. A. 1992, *A&A*, 254, 436
- Casini, R., & Judge, P. G. 1999, *ApJ*, 522, 524 (erratum 533, 574 [2000])
- Charvin, P. 1965, *Ann. d'Astrophys.*, 28, 877
- Darnell, T., Tomczyk, S., Card, G., Judge, P. G., Casini, R., & Burkepile, J. 2003, in *AGU Fall Meeting Abstracts* (Washington, DC: AGU), B505
- Dere, K. P., Landi, E., Young, P. R., & Del Zanna, G. 2001, *ApJS*, 134, 331
- Flower, D. R., & Pineau des Forêts, G. 1973, *A&A*, 24, 181
- Fong, B., Low, B. C., & Fan, Y. 2002, *ApJ*, 571, 987
- Gilbert, H. R., Holzer, T. E., & MacQueen, R. M. 2005, *ApJ*, 618, 524
- Golub, L., et al. 1999, *Phys. Plasmas*, 6, 2205
- Gopalswamy, N., & Hanaoka, Y. 1998, *ApJ*, 498, L179
- Harvey, J. W. 1969, Ph.D. thesis, Univ. Colorado
- House, L. L. 1972, *Sol. Phys.*, 23, 103
- . 1974, *PASP*, 86, 490
- . 1977, *ApJ*, 214, 632
- Illing, R. M. E., & Hundhausen, A. J. 1986, *J. Geophys. Res.*, 91(A10), 10951
- Jordan, C. 1969, *MNRAS*, 142, 501
- Judge, P., Casini, R., Tomczyk, S., Edwards, D. P., & Francis, E. 2001, *Coronal Magnetometry: A Feasibility Study* (Tech. Rep. NCAR/TN-446-STR; Boulder: NCAR)
- Judge, P. G. 1998, *ApJ*, 500, 1009
- Judge, P. G., & Casini, R. 2001, in *ASP Conf. Ser.* 236, *Advanced Solar Polarimetry: Theory, Observation, and Instrumentation*, ed. M. Sigwarth (San Francisco: ASP), 503
- Landi degl'Innocenti, E., & Landolfi, M. 2004, *Polarization in Spectral Lines* (Dordrecht: Kluwer)
- Landman, D. A. 1975, *A&A*, 43, 285
- Leroy, J. L. 1989, in *Dynamics and Structure of Quiescent Solar Prominences*, ed. E. R. Priest (Dordrecht: Kluwer), 77
- Lin, H., Kuhn, J. R., & Coulter, R. 2004, *ApJ*, 613, L177
- Lin, H., Penn, M. J., & Tomczyk, S. 2000, *ApJ*, 541, L83
- Lites, B. W. 2005, *ApJ*, 622, 1275
- Low, B. C. 1994, *Phys. Plasmas* 1(5), 1684
- . 2003, in *ASP Conf. Ser.* 286, *Current Theoretical Models and Future High Resolution Solar Observations: Preparing for ATST*, ed. A. A. Pevtsov & H. Uitenbroek (San Francisco: ASP), 335
- Low, B. C., Fong, B., & Fan, Y. 2003, *ApJ*, 594, 1060
- Pecker, J. C., & Thomas, R. N. 1962, *Ann. d'Astrophys.*, 25, 100
- Penn, M. J., & Kuhn, J. R. 1994, *ApJ*, 434, 807
- Penn, M. J., Kuhn, J. R., Arnaud, J., Mickey, D. L., & Labonte, B. J. 1994, *Space Sci. Rev.*, 70, 185
- Querfeld, C. 1977, *Proc. SPIE*, 112, 200
- . 1982, *ApJ*, 255, 764
- Querfeld, C. W., & Smartt, R. N. 1984, *Sol. Phys.*, 91, 299
- Sahal-Bréchet, S. 1974a, *A&A*, 32, 147
- . 1974b, *A&A*, 36, 355
- . 1977, *ApJ*, 213, 887
- Smart, R., Dunn, R. B., & Fisher, R. R. 1981, *Proc. SPIE*, 288, 395
- Taylor, J. B. 1986, *Rev. Mod. Phys.*, 58, 741
- Tomczyk, S. 2003, in *AGU Fall Meeting Abstracts* (Washington, DC: AGU), D3
- . 2004, in *AGU Fall Meeting Abstracts* (Washington, DC: AGU), B4
- Tomczyk, S., Card, G. L., Darnell, T., Elmore, D. F., Casini, R., Judge, P. G., & Burkepile, J. 2004, *BAAS*, 36, 686
- White, S. M. 2001, in *ASP Conf. Ser.* 248, *Magnetic Fields across the Hertzsprung-Russell Diagram*, ed. G. Mathys, S. Solanki, & D. Wickramasinghe (San Francisco: ASP), 67
- Zhang, M., & Low, B. 2004, *ApJ*, 600, 1043
- . 2005, *ARA&A*, 43, 103